FFT-based bounds on the permeability of complex microstructures

François Bignonnet, Luc Dormieux

INTERNATIONAL JOURNAL FOR NUMERICAL AND ANALYTICAL METHODS IN GEOMECHANICS
Int. J. Numer. Anal. Meth. Geomech. 2014; **38**:1707–1723
Published online in Wiley InterScience (www.interscience.wiley.com). DOI: 10.1002/nag.2278

FFT-based bounds on the permeability of complex microstructures

F. Bignonnet*; L. Dormieux

Université Paris-Est, UR Navier, Ecole des Ponts ParisTech, 6-8 Av. Blaise Pascal, Cité Descartes, Champs-sur-Marne, F-77455 Marne-La-Vallée Cedex 2, France

SUMMARY

A numerical scheme for the computation of the permeability of complex microstructures is presented. As a darcean counterpart of the FFT-based scheme in elasticity, the method is designed to be directly coupled with 3D imaging techniques of porous samples, without meshing or definition of an equivalent pore network. The method relies on the variational principle of Hashin and Shtrikman which ensures a rigorous upper bound status to the estimated permeabilities and provides an energetically consistent rule for heterogeneous voxels comprising both the solid and fluid phases.

Received ...

KEY WORDS: Permeability; Numerical homogenization; Fast Fourier Transform; Variational framework; Polarization

1. INTRODUCTION

In a pioneering work, [1] early clarified the theoretical link between the macroscopic Darcy's law for fluid flow in porous media and the microscopic Stokes flow within the pore space. Furthermore, this approach provided a mean to determine the permeability tensor, at least theoretically, as a function of the geometry of the pore space at the microscopic scale. A quantitatively precise prediction of the permeability of porous media thus requires an accurate description of the pore geometry.

Within this framework, successful predictions of the permeability of idealized regular-shaped granular materials have been derived [2, 3], but the authors warned for their application to other types of materials. To further capture the complexity of pore space geometry, pore-networks models idealizing real microstructures may be finely constructed from images of the pore space [4], and were shown to provide good estimates of both single and multi-phase flow.

*Correspondence to: Université Paris-Est, UR Navier, Ecole des Ponts ParisTech, 6-8 Av. Blaise Pascal, Cité Descartes, Champs-sur-Marne, F-77455 Marne-La-Vallée Cedex 2, France. E-mail: francois.bignonnet@enpc.fr

A more accurate description of the fluid flow requires direct full field simulations on real pore geometries. The recent advances in imaging techniques allow precise reconstruction of the microstructure down to a few nanometers [5]. Most methods are based on approximate solutions of Stokes equations in the pore space. Finite elements simulations are hindered by the complex stage of meshing real microstructures. Therefore alternate numerical methods have been developed to be directly compatible with imaging techniques. Lattice Boltzmann methods have been used to compute the intrinsic and relative permeabilities of rock samples [6], but are computationally intensive and are still limited to relatively small systems, even using parallelized algorithms on modern Graphical Processor Units. Finite volume based methods have been used [7] but are still rather slow.

In order to accelerate computations, alternate schemes have been proposed using periodic boundary conditions and taking advantage of the fast evaluation of non local terms by FFT. An adaptation of Peskin's Immersed Boundary Method based on finite differences on staggered discretization grids has been proposed [8] and proves to dramatically improve computational time.

Another fruitful approach is the adaptation of the FFT-based scheme initially introduced in linear elasticity [9]. This scheme was designed to be directly interfaced with imaging techniques and has been adapted to permeability [10]. Since then, a variational FFT-based scheme has been introduced in linear elasticity [11], improving the performances of the so-called basic scheme [9]. It consists in the minimization of an energy Hashin-Shtrikman functional, allowing for an energetically consistent way of dealing with heterogeneous voxels and providing rigorous bounds of the homogenized properties. Recent advances [12] made it fairly simple to implement and suitable for computations on large discretization grids.

The present paper proposes a numerical scheme for the computation of permeability inspired from the Hashin and Shtrikman based FFT scheme. In section 2, the framework of the homogenization of periodic media is recalled in the context of permeability, with a specific focus on its variational formulation. The latter is linked with the Hashin and Shtrikman formulation described in section 3 and an energetically consistent discretization is derived. A validation of the method is proposed on simple geometries in section 4 by comparison with finite element simulations and literature results.

2. BACKGROUND: THE INITIAL FLUID FLOW MICROMECHANICAL PROBLEM

At the macroscopic scale, Darcy's law linearly relates the pressure gradient $\boldsymbol{\alpha}$ to the fluid velocity $\boldsymbol{V}$ through the permeability tensor by $\boldsymbol{V} = -\boldsymbol{K} \cdot \boldsymbol{\alpha}$.

A micromechanical approach to permeability has initially been presented by Ene and Sanchez-Palencia [1] in the context of periodic boundary conditions. The elementary cell Ω is a rectangular parallelepiped of boundary $\partial\Omega$, comprising a non deformable solid phase in Ω_s and a pore space Ω_f filled with an incompressible Newtonian fluid of viscosity μ. The porosity of the elementary cell is $\varphi = \frac{|\Omega_f|}{|\Omega|}$. The spacial coordinates at the micro scale are denoted by $\boldsymbol{z}$. In this initial problem (P^i), the fluid flow is described by the pressure field $p^i(\boldsymbol{z})$ and the velocity field $\boldsymbol{v}^i(\boldsymbol{z})$ in Ω_f.

According to the separation of scale principle [2, 13], the fluid is loaded by the macroscopic pressure gradient $\boldsymbol{\alpha}$ which is equal to the volume average over Ω of the microscopic pressure gradient, by considering an extension of the pressure field to the solid phase. The pressure field may thus be rewritten in both fluid and solid phases $p^i(\boldsymbol{z}) = \boldsymbol{\alpha} \cdot \boldsymbol{z} + \phi^i(\boldsymbol{z})$ where $\phi^i(\boldsymbol{z})$ is a periodic pressure fluctuation at the micro-scale.

The velocity field has to comply with several kinematic conditions:

- no-slip boundary condition at the solid-fluid interface $\mathcal{I}_{sf}$,
- periodic boundary conditions on $\partial\Omega \cap \Omega_f$,
- incompressibility or continuity equation $\operatorname{div}(\boldsymbol{v^i}) = 0$ in Ω_f.

DOI: 10.1002/nag.2278

The initial set $\mathcal{C}^i$ of kinematically admissible velocity fields $\boldsymbol{u}$ is thus

$$\mathcal{C}^i = \{\boldsymbol{u} \mid \boldsymbol{u} \text{ periodic on } \partial\Omega \cap \Omega_f, \boldsymbol{u}(\boldsymbol{z}) = \boldsymbol{0} \text{ on } \mathcal{I}_{sf} \\ \operatorname{div}(\boldsymbol{u}) = 0 \text{ on } \Omega_f\}.$$

For the initial problem (P^i), local equations read

$$\boldsymbol{v^i} \in \mathcal{C}^i, \tag{1a}$$

$$2\boldsymbol{d^i}(\boldsymbol{z}) = \mathbf{grad}(\boldsymbol{v^i}(\boldsymbol{z})) +^t \mathbf{grad}(\boldsymbol{v^i}(\boldsymbol{z})) \quad (\boldsymbol{z} \in \Omega_f), \tag{1b}$$

$$\boldsymbol{\sigma^i}(\boldsymbol{z}) = 2\mu\, \boldsymbol{d^i}(\boldsymbol{z}) - \left(\boldsymbol{\alpha} \cdot \boldsymbol{z} + \phi^i(\boldsymbol{z})\right) \boldsymbol{I} \quad (\boldsymbol{z} \in \Omega_f), \tag{1c}$$

$$\mathbf{div}(\boldsymbol{\sigma^i}(\boldsymbol{z})) = \boldsymbol{0} \quad (\boldsymbol{z} \in \Omega_f), \tag{1d}$$

where $\boldsymbol{d^i}(\boldsymbol{z})$ is the strain rate deriving from the velocity $\boldsymbol{v^i}(\boldsymbol{z})$ (eq. 1b), related to the stress $\boldsymbol{\sigma^i}(\boldsymbol{z})$ by the Newtonian behavior (eq. 1c). For Stokes flows, the inertia effects in the momentum balance are neglected (eq. 1d).

The problem (P^i) is linear with respect to the loading parameter $\boldsymbol{\alpha}$, so that the velocity field depends on $\boldsymbol{\alpha}$ through a localization tensor $\boldsymbol{k(z)}$

$$\boldsymbol{v^i}(\boldsymbol{z}) = -\boldsymbol{k}(\boldsymbol{z}) \cdot \boldsymbol{\alpha}.$$

Besides, the macroscopic velocity relates to the microscopic velocity through

$$\boldsymbol{V} = \varphi \overline{\boldsymbol{v^i}}^f = -\varphi \overline{\boldsymbol{k}}^f \cdot \boldsymbol{\alpha},$$

where the following notation is being used for any domain Ω_j

$$\overline{u}^j = \frac{1}{|\Omega_j|} \int_{\Omega_j} u(\boldsymbol{z})\, \mathrm{d}\, V_z.$$

Darcy's law is recognized and the permeability tensor appears as

$$\boldsymbol{K} = \varphi \overline{\boldsymbol{k}}^f.$$

Hence, the resolution of (P^i) directly provides the permeability tensor.

For practical implementations, a classical approach to derive approximate solutions of (P^i) is the use of a variational framework. For a given strain rate $\boldsymbol{d}$, the density of dissipated energy due to viscosity is $w(\boldsymbol{d}) = \mu\, \boldsymbol{d} : \boldsymbol{d}$. Following [14, 15], the variational formulation of (P^i) is

$$-\frac{1}{2}\boldsymbol{\alpha} \cdot \boldsymbol{K} \cdot \boldsymbol{\alpha} = \inf_{\boldsymbol{u} \in \mathcal{C}^i} \left(\frac{1}{|\Omega|} \int_{\Omega_f} w(\boldsymbol{d}(\boldsymbol{u})) + \boldsymbol{\alpha} \cdot \boldsymbol{u}\, \mathrm{d}\, V_z \right). \tag{2}$$

For any choice of a kinematically admissible velocity field, (2) provides a lower bound estimate of the permeability. Akin to the minimum of potential energy in linear elasticity, this inequality is the basis for finite element methods, which explore subsets of $\mathcal{C}^i$ with finite dimension (see e.g. [16]). However, the no-slip boundary condition requires a precise description of the solid fluid interphase. Indeed, problem (P^i) is defined on the pore space Ω_f only. A complex meshing procedure has thus to be carried out, which is time consuming and difficult to implement in the case of real microstructures. Therefore, it is desirable derive another variational principle in order to get rid of boundary conditions in the space of test function $\mathcal{C}^i$. This is the purpose of the next section.

DOI: 10.1002/nag.2278

3. VARIATIONAL PERSPECTIVE OF FOURIER-BASED METHODS IN FLUID FLOWS

3.1. An extended flow problem

The idea is to define a boundary value problem on the whole elementary cell instead of the pore space only. To do so, the rigid solid can be regarded as an incompressible viscous fluid with an infinite viscosity. The essential advantage of this point of view lies in the fact that the no-slip boundary condition at the solid-fluid interface vanishes and will be automatically met by the solution to the problem.

The proposed idea however presents a shortcoming: the rigid body motions of the solid domain must be prevented, or it would simply be dragged by the fluid.

Since the proposed method aims at dealing with real microstructures, solid phases with disjoint domains are not considered. Furthermore, periodicity implies that rotation may not occur if the solid phase spans over the whole cell. Hence only a no-velocity condition will be considered, either (i) in a single point of the solid phase, or (ii) in average over any subdomain included in the solid phase. Note that in the case of a single solid particle isolated in the fluid phase, rotation is not prevented. At this stage, more complex conditions to prevent rotation or deal with multiple particles could be added but would imply a more involved treatment in the sequel, although the main ideas would remain valid.

The following developments focus on choice (ii), for any subdomain $\Omega_{\mathcal{S}} \subset \Omega_s$ whose volume fraction $f_{\mathcal{S}} = \frac{|\Omega_{\mathcal{S}}|}{|\Omega|}$ is not null. Considerations in this section lead to the definition of a simplified set $\mathcal{C}$ of kinematically admissible velocity fields $\boldsymbol{u}$ for the new extended problem (P) defined on the whole elementary cell Ω

$$\mathcal{C} = \{\boldsymbol{u} \mid \boldsymbol{u} \text{ periodic on } \partial\Omega, \overline{\boldsymbol{u}}^{\mathcal{S}} = \boldsymbol{0}, \operatorname{div}(\boldsymbol{u}) = 0 \text{ on } \Omega_f\}.$$

The dual quantity (or Lagrange multiplier) associated to this no-velocity condition is a uniform body force applied on $\Omega_{\mathcal{S}}$. In this specific case where only one no-velocity condition is chosen, the Lagrange multiplier is known.

Indeed, according to [2], momentum balance states that macroscopic stresses in the solid phase counterbalance the macroscopic fluid pressure gradient. These macroscopic stresses may microscopically be considered as body forces $\boldsymbol{\lambda}$ in the solid phase. For the sake of clarity, a subscript f (resp. s) is adopted in the following reasoning for all quantities defined in the fluid (resp. solid) phase. $\boldsymbol{n}_i$ denotes the unit normal of the surface $\partial\Omega_i$, oriented towards the outside of the domain Ω_i.

Integration of the momentum balance in the fluid phase writes

$$\int_{\Omega_f} \mathbf{div}\, \boldsymbol{\sigma}_f \,\mathrm{d}\, V_z = \int_{\partial\Omega_f} \boldsymbol{\sigma}_f \cdot \boldsymbol{n}_f \,\mathrm{d}\, S_z = \boldsymbol{0}.$$

The surface $\partial\Omega_f$ may be split in $\mathcal{I}_{sf}$ and $\partial\Omega \cap \Omega_f$. Use of the periodic boundary conditions on the second part leads to

$$\int_{\mathcal{I}_{sf}} \boldsymbol{\sigma}_f \cdot \boldsymbol{n}_f \,\mathrm{d}\, S_z - \int_{\partial\Omega\cap\Omega_f} \boldsymbol{\alpha}\cdot\boldsymbol{z}\, \boldsymbol{n}_f \,\mathrm{d}\, S_z = \boldsymbol{0}. \tag{3}$$

Similarly, remembering that the pressure in the solid has been defined with a linear part in $\boldsymbol{\alpha}$ and a periodic fluctuation, integration of the momentum balance in the solid phase writes

$$\begin{aligned} \boldsymbol{0} &= \int_{\Omega_s} \boldsymbol{\lambda} + \mathbf{div}\, \boldsymbol{\sigma}_s \,\mathrm{d}\, V_z \\ &= \int_{\Omega_s} \boldsymbol{\lambda} \,\mathrm{d}\, V_z + \int_{\mathcal{I}_{sf}} \boldsymbol{\sigma}_s \cdot \boldsymbol{n}_s \,\mathrm{d}\, S_z - \int_{\partial\Omega\cap\Omega_s} \boldsymbol{\alpha}\cdot\boldsymbol{z}\, \boldsymbol{n}_s \,\mathrm{d}\, S_z. \end{aligned} \tag{4}$$

On $\mathcal{I}_{sf}$, the normals $\boldsymbol{n}_s$ and $\boldsymbol{n}_f$ are opposite, whereas they are equal on $\partial\Omega$. Summing (3) and (4) gives

$$\int_{\Omega_s} \boldsymbol{\lambda} \,\mathrm{d}\, V_z + \int_{\mathcal{I}_{sf}} (\boldsymbol{\sigma}_s - \boldsymbol{\sigma}_f)\cdot \boldsymbol{n}_s \,\mathrm{d}\, S_z = \int_{\partial\Omega} \boldsymbol{\alpha}\cdot\boldsymbol{z}\, \boldsymbol{n} \,\mathrm{d}\, S_z.$$

Prepared using nagauth.cls
DOI: 10.1002/nag.2278

Stress continuity at the solid-fluid interface causes the first surface integral to vanish, so that the body forces $\boldsymbol{\lambda}$ are known in average

$$\int_{\Omega_s} \boldsymbol{\lambda} \, \mathrm{d}\, V_z = |\Omega| \boldsymbol{\alpha}.$$

As both deformation and displacement are null in the solid phase, any choice of external force equilibrating the macroscopic pressure gradient will result in no additional work. As previously stated, the Lagrange multiplier of the no-velocity boundary condition on average over $\Omega_{\mathcal{S}}$ is an additional uniform body force applied on $\Omega_{\mathcal{S}}$. Previous momentum balance imposes this body force to be $f_{\mathcal{S}}^{-1}\boldsymbol{\alpha}$.

The field equations of the new extended problem (P) defined on the whole elementary cell Ω read

$$\boldsymbol{v} \in \mathcal{C},$$

$$2\boldsymbol{d}(\boldsymbol{z}) = \mathbf{grad}(\boldsymbol{v}(\boldsymbol{z})) +^t \mathbf{grad}(\boldsymbol{v}(\boldsymbol{z})) \quad (\boldsymbol{z} \in \Omega),$$

$$\mathbf{div}(\boldsymbol{\sigma}(\boldsymbol{z})) = \begin{cases} -f_{\mathcal{S}}^{-1}\boldsymbol{\alpha} & \text{if } \boldsymbol{z} \in \Omega_{\mathcal{S}}, \\ \mathbf{0} & \text{otherwise,} \end{cases}$$

$$\boldsymbol{\sigma}(\boldsymbol{z}) = 2\mu(\boldsymbol{z})\, \boldsymbol{d}(\boldsymbol{z}) - (\boldsymbol{\alpha} \cdot \boldsymbol{z} + \phi(\boldsymbol{z}))\, \boldsymbol{I} \quad (\boldsymbol{z} \in \Omega),$$

$$\text{with } \mu(\boldsymbol{z}) = \begin{cases} \infty & \text{if } \boldsymbol{z} \in \Omega_s, \\ \mu & \text{if } \boldsymbol{z} \in \Omega_f. \end{cases}$$

The unknowns of problem (P) are the velocity field $\boldsymbol{v}$ and the stress field $\boldsymbol{\sigma}$ or, in an equivalent manner, $\boldsymbol{v}$ and the periodic pressure fluctuation ϕ.

These equations are formally identical to a problem of heterogeneous elasticity involving two incompressible phases. We therefore could expect to take advantage of the homogenization methods developed in solid micromechanics. However this analogy breaks down when the boundary conditions and loading parameters are considered. In solid micromechanics, the loading parameter is the macroscopic strain tensor, which defines boundary conditions as an affine displacement with periodic fluctuations. Here, the loading parameter of problem (P) is the macroscopic pressure gradient vector associated to its equilibrating body forces in $\Omega_{\mathcal{S}}$.

Nevertheless, we shall see later that seminal ideas of solid micromechanics will be of great help in the present context of fluid flow. The next step is to derive the variational formulation of (P).

3.2. Variational formulation of the extended problem

Following [14], the variational formulation of (P) consists in integrating over Ω the product of the momentum balance equation by a kinematically admissible test function $\boldsymbol{u} \in \mathcal{C}$

$$\forall \boldsymbol{u} \in \mathcal{C}, \int_{\Omega} \boldsymbol{u} \cdot \mathbf{div}(\boldsymbol{\sigma}) \, \mathrm{d}\, V_z = 0,$$

where the body forces in $\Omega_{\mathcal{S}}$ do not work because of the no-velocity condition. Use of the divergence theorem leads to

$$\int_{\Omega} \boldsymbol{u} \cdot \mathbf{div}(\boldsymbol{\sigma}) \, \mathrm{d}\, V_z = -\int_{\Omega} \boldsymbol{d}(u) : \boldsymbol{\sigma} \, \mathrm{d}\, V_z + \int_{\partial\Omega} \boldsymbol{u} \cdot \boldsymbol{\sigma} \cdot \boldsymbol{n} \, \mathrm{d}\, S_z.$$

Then, taking advantage of the periodicity of $\boldsymbol{u}$, $\boldsymbol{v}$ and ϕ together with the condition $\mathrm{tr}\, \boldsymbol{d}(\boldsymbol{u}) = \mathrm{div}\, \boldsymbol{u} = 0$ yields

$$0 = -\int_{\Omega} 2\mu\, \boldsymbol{d}(u) : \boldsymbol{d}(v) \, \mathrm{d}\, V_z - \int_{\partial\Omega} \boldsymbol{u} \cdot (\boldsymbol{\alpha} \cdot \boldsymbol{z}) \cdot \boldsymbol{n} \, \mathrm{d}\, S_z.$$

Prepared using nagauth.cls
DOI: 10.1002/nag.2278

Introducing the bilinear definite positive form $\mathcal{A}(\boldsymbol{u},\boldsymbol{v}) = \overline{2\mu\,\boldsymbol{d}(u):\boldsymbol{d}(v)}$ provides the weak formulation of (P)

$$\forall \boldsymbol{u} \in \mathcal{C}, \mathcal{A}(\boldsymbol{u},\boldsymbol{v}) = -\boldsymbol{\alpha}\cdot\overline{\boldsymbol{u}}.$$

Combining this result for the solution velocity $\boldsymbol{v}$ with the definition of the permeability tensor provides the identity

$$\frac{1}{2}\mathcal{A}(\boldsymbol{v},\boldsymbol{v}) = \overline{w\left(\boldsymbol{d}(\boldsymbol{v})\right)} = -\frac{1}{2}\boldsymbol{\alpha}\cdot\boldsymbol{K}\cdot\boldsymbol{\alpha}.$$

Let us introduce the functional $\mathcal{F}$ defined on $\mathcal{C}$ by

$$\mathcal{F}(\boldsymbol{u}) = \frac{1}{2}\mathcal{A}(\boldsymbol{u},\boldsymbol{u}) + \boldsymbol{\alpha}\cdot\overline{\boldsymbol{u}}.$$

For all $\boldsymbol{u}\in\mathcal{C}$, the field $\boldsymbol{\partial v} = \boldsymbol{u}-\boldsymbol{v} \in \mathcal{C}$ and

$$\mathcal{F}(\boldsymbol{u}) = \mathcal{F}(\boldsymbol{v}) + \frac{1}{2}\mathcal{A}(\boldsymbol{\partial v},\boldsymbol{\partial v}) + \mathcal{A}(\boldsymbol{\partial v},\boldsymbol{v}) + \boldsymbol{\alpha}\cdot\overline{\boldsymbol{\partial v}}.$$

Applying the weak formulation of (P) to $\boldsymbol{\partial v}$

$$\forall \boldsymbol{u}\in\mathcal{C}, \mathcal{F}(\boldsymbol{u}) = \mathcal{F}(\boldsymbol{v}) + \frac{1}{2}\mathcal{A}(\boldsymbol{\partial v},\boldsymbol{\partial v}) \geq \mathcal{F}(\boldsymbol{v}).$$

This results implies the functional $\mathcal{F}$ is minimum in $\mathcal{C}$ for the solution $\boldsymbol{v}$ of (P). A lower bound estimate of the permeability $\boldsymbol{K}$ is obtained for any choice of a test function $\boldsymbol{u}\in\mathcal{C}$ and it follows

$$-\frac{1}{2}\boldsymbol{\alpha}\cdot\boldsymbol{K}\cdot\boldsymbol{\alpha} = \inf_{\boldsymbol{u}\in\mathcal{C}}\left(\overline{w(\boldsymbol{d}(\boldsymbol{u})) + \boldsymbol{\alpha}\cdot\boldsymbol{u}}\right) \leq \frac{1}{2}\mathcal{A}(\boldsymbol{u},\boldsymbol{u}) + \boldsymbol{\alpha}\cdot\overline{\boldsymbol{u}}. \tag{6}$$

This variational result (6) is similar to (2), but defined on the extended set of kinematically admissible fields $\mathcal{C}$. Direct use of this variational principle (e.g. FEM) is numerically difficult because of the infinite contrast in viscosity and the incompressibility condition. In the following section, (6) will be used to derive a Hashin and Shtrikman variational principle [17], in which the so-called polarization field to optimize has no condition to fulfill. Another motivation is that the optimization problem associated with the Hashin and Shtrikman variational principle is known in solid micromechanics to lead to a FFT scheme able to deal with infinite contrast [11].

3.3. Hashin and Shtrikman variational framework

In the line of reasoning of [18], a transposition of the Hashin and Shtrikman variational principle [17] to darcean homogenization may be derived. The main idea is to transfer the difficulty arising from a heterogeneity in viscosity to an additional loading parameter $\boldsymbol{\tau}$, called polarization, which may be thought of as a prestress.

The Legendre transform of the density of dissipated energy $w(\boldsymbol{d})$ is defined on the space of stress tensors as

$$w^*(\boldsymbol{\tau}) = \sup_{\boldsymbol{d}}\left(\boldsymbol{\tau}:\boldsymbol{d}(\boldsymbol{u}) - w(\boldsymbol{d})\right). \tag{7}$$

In elasticity, the Legendre transform defines the stress elastic energy. In the case of an incompressible isotropic Newtonian fluid, (7) solves to $w^*(\boldsymbol{\tau}) = (4\mu)^{-1}\boldsymbol{\tau}:\boldsymbol{\tau}$.

Let us consider a reference medium of uniform viscosity μ_0 smaller than any local value of the viscosity in the heterogeneous medium at hand. According to its definition, the Legendre transform $(w-w_0)^*$ associated with a heterogeneous medium of viscosity $\mu(\boldsymbol{z})-\mu_0$ satisfies

$$\forall\boldsymbol{\tau};\forall\boldsymbol{d};w(\boldsymbol{d}) \geq w_0(\boldsymbol{d}) + \boldsymbol{\tau}:\boldsymbol{d} - (w-w_0)^*(\boldsymbol{\tau}).$$

After addition of the loading term in $\boldsymbol{\alpha}$ and volume averaging over Ω, the minimum over all kinematically admissible velocity fields in $\mathcal{C}$ yields

$$\begin{aligned}\forall\boldsymbol{\tau};-\frac{1}{2}\boldsymbol{\alpha}\cdot\boldsymbol{K}\cdot\boldsymbol{\alpha} = \inf_{\boldsymbol{u}\in\mathcal{C}}\left(\overline{w(\boldsymbol{d}(\boldsymbol{u})) + \boldsymbol{\alpha}\cdot\boldsymbol{u}}\right) \geq \\ \inf_{\boldsymbol{u}\in\mathcal{C}}\left(\overline{w_0(\boldsymbol{d}(\boldsymbol{u})) + \boldsymbol{\tau}:\boldsymbol{d}(\boldsymbol{u}) + \boldsymbol{\alpha}\cdot\boldsymbol{u}}\right) - \overline{(w-w_0)^*(\boldsymbol{\tau})}.\end{aligned} \tag{8}$$

DOI: 10.1002/nag.2278

The result (8) is known as the Hashin Shtrikman variational principle [17]. The left term corresponds to the variational formulation (6) of (P). The first part of the right term is the variational formulation of an auxiliary problem (P^0) similar to (P), except the viscosity is homogeneous and the polarization field is an additional loading parameter. The second part is known by definition of the Legendre transform. The whole right hand side is a functional of the variable $\boldsymbol{\tau}$ called Hashin and Shtrikman functional $\mathcal{HS}(\boldsymbol{\tau})$. The equality is met for a unique optimum polarization field, solution of the Lippmann Schwinger equation. The inequality (8) is the basis of the proposed FFT scheme since it may be used to provide upper bound estimates of the permeability for *any choice* of a polarization field $\boldsymbol{\tau}$, with *no condition* on $\boldsymbol{\tau}$.

3.4. Auxiliary problems

In order to fully express the quadratic dependence on $\boldsymbol{\tau}$ of the Hashin and Shtrikman functional, the following auxiliary problem (P^0) has to be solved

$$\boldsymbol{v}^0 \in \mathcal{C},$$

$$2\boldsymbol{d}^0(\boldsymbol{z}) = \mathbf{grad}(\boldsymbol{v}^0(\boldsymbol{z})) +^t \mathbf{grad}(\boldsymbol{v}^0(\boldsymbol{z})) \quad (\boldsymbol{z} \in \Omega),$$

$$\boldsymbol{\sigma}^0(\boldsymbol{z}) = 2\mu_0\, \boldsymbol{d}^0(\boldsymbol{z}) - \left(\boldsymbol{\alpha}\cdot\boldsymbol{z} + \phi^0(\boldsymbol{z})\right)\boldsymbol{I} + \boldsymbol{\tau} \quad (\boldsymbol{z} \in \Omega),$$

$$\mathbf{div}(\boldsymbol{\sigma}^0(\boldsymbol{z})) = \begin{cases} -f_{\mathcal{S}}^{-1}\boldsymbol{\alpha} & \text{if } \boldsymbol{z} \in \Omega_{\mathcal{S}}, \\ \mathbf{0} & \text{otherwise.} \end{cases}$$

The Hashin and Shtrikman functional is then expressed as

$$\mathcal{HS}(\boldsymbol{\tau}) = \overline{w_0(\boldsymbol{d}^0) + \boldsymbol{\tau} : \boldsymbol{d}^0} + \boldsymbol{\alpha}\cdot\overline{\boldsymbol{u}^0} - \overline{(w - w_0)^*(\boldsymbol{\tau})}.$$

(P^0) may conveniently be split using superposition in a so called reference problem (P^α) loaded only by the macroscopic pressure gradient $\boldsymbol{\alpha}$ by setting $\boldsymbol{\tau}$ to zero in (P^0) and a problem (P^τ) loaded only by the polarization field $\boldsymbol{\tau}$ by setting $\boldsymbol{\alpha}$ to zero in (P^0). In the following developments, exponent α (resp. τ) refers to the solution of (P^α) (resp. (P^τ)).

The Hashin and Shtrikman functional is simplified by repeatedly using the divergence theorem and boundary conditions to

$$\mathcal{HS}(\boldsymbol{\tau}) = \frac{1}{2}\boldsymbol{\alpha}\cdot\overline{\boldsymbol{v}^\alpha} + \overline{\boldsymbol{d}^\alpha : \boldsymbol{\tau}} + \frac{1}{2}\overline{\boldsymbol{\tau} : \boldsymbol{d}^\tau} - \frac{1}{2}\overline{(2\mu - 2\mu_0)^{-1}\boldsymbol{\tau} : \boldsymbol{\tau}}. \tag{10}$$

Since the viscosity is uniform in both sub problems, they may be solved using Green operators. The solution of problem (P^α) is expressed thanks to the Green function $\boldsymbol{G}_0$ and the transpose of the third order Green operator $\boldsymbol{\mathcal{G}}_0$ of the reference medium defined in A.

$$\boldsymbol{v}^\alpha(\boldsymbol{z}) = \overline{\boldsymbol{v}^\alpha} + \left(\boldsymbol{G}_0 * f_{\mathcal{S}}^{-1}\chi^{\mathcal{S}}\boldsymbol{\alpha}\right)(\boldsymbol{z}),$$

$$\boldsymbol{d}^\alpha(\boldsymbol{z}) = \left({}^t\boldsymbol{\mathcal{G}}_0 * f_{\mathcal{S}}^{-1}\chi^{\mathcal{S}}\boldsymbol{\alpha}\right)(\boldsymbol{z}).$$

Similarly, the solution of problem (P^τ) is expressed thanks to the third order Green operator $\boldsymbol{\mathcal{G}}_0$ and the classical fourth order Green operator $\boldsymbol{\Gamma}_0$ of the reference medium

$$\boldsymbol{v}^\tau(\boldsymbol{z}) = \overline{\boldsymbol{v}^\tau} + \left(\boldsymbol{\mathcal{G}}_0 * \boldsymbol{\tau}\right)(\boldsymbol{z}),$$

$$\boldsymbol{d}^\tau(\boldsymbol{z}) = -\left(\boldsymbol{\Gamma}_0 * \boldsymbol{\tau}\right)(\boldsymbol{z}).$$

The average velocities in both problems may be computed thanks to the no velocity boundary condition, namely for problem (P^α)

$$\overline{\boldsymbol{v}^\alpha\chi^{\mathcal{S}}} = 0 = \overline{\overline{\boldsymbol{v}^\alpha}\chi^{\mathcal{S}}} + \overline{\chi^{\mathcal{S}}\left(\boldsymbol{G}_0 * f_{\mathcal{S}}^{-1}\chi^{\mathcal{S}}\right)}\cdot\boldsymbol{\alpha},$$

Prepared using nagauth.cls
DOI: 10.1002/nag.2278

where the auto-influence term of the Green function over $\Omega_{\mathcal{S}}$ is recognized (see Appendix C). Finally,

$$\overline{\boldsymbol{v}^{\alpha}} = -\boldsymbol{G}_0^{\mathcal{S}\mathcal{S}} \cdot \boldsymbol{\alpha}.$$

The auto-influence term $\boldsymbol{G}_0^{\mathcal{S}\mathcal{S}}$ may thus be considered as the permeability of the fictitious reference problem (P^{α}). The Hashin and Shtrikman functional may now be explicited as a quadratic form in $\boldsymbol{\tau}$, and the upper bound on the permeability writes

$$\begin{aligned} \forall \boldsymbol{\tau}, \frac{1}{2}\boldsymbol{\alpha}\cdot\boldsymbol{K}\cdot\boldsymbol{\alpha} \leqslant & \frac{1}{2}\boldsymbol{\alpha}\cdot\boldsymbol{G}_0^{\mathcal{S}\mathcal{S}}\cdot\boldsymbol{\alpha} - \overline{\left({}^t\boldsymbol{\mathcal{G}}_0 * f_{\mathcal{S}}^{-1}\chi^{\mathcal{S}}\boldsymbol{\alpha}\right):\boldsymbol{\tau}} \\ & + \frac{1}{2}\overline{\boldsymbol{\tau}:\boldsymbol{\Gamma}_0*\boldsymbol{\tau}} + \frac{1}{2}\overline{(2\mu-2\mu_0)^{-1}\boldsymbol{\tau}:\boldsymbol{\tau}}. \end{aligned} \tag{13}$$

3.5. Application to voxel-wise constant polarization field

The d-dimensional domain Ω is divided in a regular $N_1 \times ... \times N_d$ grid of $N = N_1...N_d$ subdomains $\Omega_{\boldsymbol{\beta}}$ (pixels for d = 2, voxels for d = 3) of length (or resolution) r along the d axis of an orthonormal basis $(\boldsymbol{e}_1, ..., \boldsymbol{e}_d)$. The multi-index $\boldsymbol{\beta} = (\beta_1, ..., \beta_d) \in \mathcal{I} = [0..N_1 - 1] \times ... \times [0..N_d - 1]$ is used to position the pixel in the d directions.

In order to optimize the Hashin and Shtrikman functional, we restrict to the exploration of the space of pixel-wise constant polarization fields. For any choice of a sequence $(\boldsymbol{\tau}_{\boldsymbol{\beta}})_{\boldsymbol{\beta}\in\mathcal{I}}$, a polarization field is associated by

$$\boldsymbol{\tau}(\boldsymbol{z}) = \sum_{\boldsymbol{\beta}\in\mathcal{I}} \boldsymbol{\tau}_{\boldsymbol{\beta}}\, \chi^{\boldsymbol{\beta}}(\boldsymbol{z}),$$

where $\chi^{\boldsymbol{\beta}}$ is the characteristic function of pixel $\Omega_{\boldsymbol{\beta}}$

$$\chi^{\boldsymbol{\beta}}(z_1\boldsymbol{e}_1 + ... + z_d\boldsymbol{e}_d) = \begin{cases} 1 & \text{if } \forall i, 2|z_i - r\beta_i| \leqslant r, \\ 0 & \text{otherwise.} \end{cases}$$

Each term of the Hashin and Shtrikman functional may be numerically computed *exactly* thanks to the consistently discretized operators introduced by [11] and briefly recalled in B. These operators allow for the use of Discrete Fourier Transforms while no truncation of the Fourier series are made. The discrete convolution products $\circledast$ are computed as a direct product in the Fourier space, using the Fast Fourier Transform (FFT) to compute the discrete Fourier transforms.

The constant term may be computed *exactly* if $\Omega_{\mathcal{S}}$ is chosen as a union of pixels, resorting to the discrete convolution product to compute the auto-interaction term

$$\boldsymbol{G}_0^{\mathcal{S}\mathcal{S}} = \frac{1}{N f_{\mathcal{S}}^2} \sum_{\boldsymbol{\beta}\in\mathcal{I}} \chi^{\mathcal{S}}_{\boldsymbol{\beta}} \left(\boldsymbol{G}_0^c \circledast \chi^{\mathcal{S}}\right)_{\boldsymbol{\beta}} = \sum_{\boldsymbol{\beta}\in\mathcal{I}} \chi^{\mathcal{S}}_{\boldsymbol{\beta}} \boldsymbol{G}_0^{\mathcal{S}\boldsymbol{\beta}}.$$

The linear term relates to the mean value of $\boldsymbol{d}^{\alpha}$ over pixel $\Omega_{\boldsymbol{\beta}}$, denoted $\boldsymbol{d}^{\alpha}_{\boldsymbol{\beta}}$, since

$$\boldsymbol{d}^{\alpha}_{\boldsymbol{\beta}} = \left({}^t\boldsymbol{\mathcal{G}}_0^c \circledast f_{\mathcal{S}}^{-1}\chi^{\mathcal{S}}\boldsymbol{\alpha}\right)_{\boldsymbol{\beta}} = \left({}^t\boldsymbol{\mathcal{G}}_0^{\boldsymbol{\beta}\mathcal{S}}\right)\cdot\boldsymbol{\alpha}.$$

The linear term is thus calculated using the relation

$$\overline{\boldsymbol{\tau}:\left({}^t\boldsymbol{\mathcal{G}}_0 * f_{\mathcal{S}}^{-1}\chi^{\mathcal{S}}\boldsymbol{\alpha}\right)} = \frac{1}{N}\sum_{\boldsymbol{\beta}\in\mathcal{I}} \boldsymbol{\tau}_{\boldsymbol{\beta}} : \left({}^t\boldsymbol{\mathcal{G}}_0^c \circledast f_{\mathcal{S}}^{-1}\chi^{\mathcal{S}}\boldsymbol{\alpha}\right)_{\boldsymbol{\beta}} = \frac{1}{N}\sum_{\boldsymbol{\beta}\in\mathcal{I}} \boldsymbol{\tau}_{\boldsymbol{\beta}} : \boldsymbol{d}^{\alpha}_{\boldsymbol{\beta}}.$$

Similarly, the first quadratic term is computed thanks to the property

$$\overline{\boldsymbol{\tau}:\boldsymbol{\Gamma}_0*\boldsymbol{\tau}} = \frac{1}{N^2}\sum_{\boldsymbol{\beta}\in\mathcal{I}}\sum_{\boldsymbol{\delta}\in\mathcal{I}} \boldsymbol{\tau}_{\boldsymbol{\beta}} : \boldsymbol{\Gamma}_0^{\boldsymbol{\beta}\boldsymbol{\delta}} : \boldsymbol{\tau}_{\boldsymbol{\delta}} = \frac{1}{N}\sum_{\boldsymbol{\beta}\in\mathcal{I}} \boldsymbol{\tau}_{\boldsymbol{\beta}} : \left(\boldsymbol{\Gamma}_0^c \circledast \boldsymbol{\tau}\right)_{\boldsymbol{\beta}},$$

Prepared using nagauth.cls
DOI: 10.1002/nag.2278

where the computation is quicker in the second option than in the first option while resorting to FFTs, by the order of magnitude $N\log(N)$ versus N^2 operations.

The second quadratic term leads to the introduction of an energetically consistent averaging rule for the equivalent viscosity of a composite pixel comprising fluid and solid. Introducing the equivalent viscosities $\mu_{\boldsymbol{\beta}}$ defined on each pixel by the averaging rule

$$(\mu_{\boldsymbol{\beta}}-\mu_0)^{-1}=N\,\overline{\chi^{\boldsymbol{\beta}}(\mu-\mu_0)^{-1}},$$

this term containing the local information may be expressed as

$$\overline{(2\mu-2\mu_0)^{-1}\boldsymbol{\tau}:\boldsymbol{\tau}}=\frac{1}{N}\sum_{\boldsymbol{\beta}\in\mathcal{I}}(2\mu_{\boldsymbol{\beta}}-2\mu_0)^{-1}\boldsymbol{\tau}_{\boldsymbol{\beta}}:\boldsymbol{\tau}_{\boldsymbol{\beta}}.$$

Gathering all these results, a bound on the permeability is obtained for any choice of the sequence $(\boldsymbol{\tau}_{\boldsymbol{\beta}})_{\boldsymbol{\beta}\in\mathcal{I}}$

$$\begin{aligned}\frac{1}{2}\boldsymbol{\alpha}\cdot\boldsymbol{K}\cdot\boldsymbol{\alpha}\leqslant&\frac{1}{2}\boldsymbol{\alpha}\cdot\boldsymbol{G}_0^{\mathcal{S}\mathcal{S}}\cdot\boldsymbol{\alpha}+\frac{1}{N}\sum_{\boldsymbol{\beta}\in\mathcal{I}}\Big(-\boldsymbol{d}^{\alpha}_{\boldsymbol{\beta}}:\boldsymbol{\tau}_{\boldsymbol{\beta}}\\&+\frac{1}{2}\left[\boldsymbol{\tau}_{\beta}:\left(\boldsymbol{\Gamma}_0^c\circledast\boldsymbol{\tau}\right)_{\boldsymbol{\beta}}+(2\mu_{\boldsymbol{\beta}}-2\mu_0)^{-1}\boldsymbol{\tau}_{\boldsymbol{\beta}}:\boldsymbol{\tau}_{\boldsymbol{\beta}}\right]\Big).\end{aligned}\tag{14}$$

The comparison of (14) with linear elasticity (Eq. (17) in [11]) shows great similarities, although the difference in loading parameter and boundary conditions lead to a more complicated reference solution: constant strain in linear elasticity versus Green operator dependent strain rate here.

Among the subset of pixel wise constant polarization fields, the optimal choice $(\boldsymbol{\tau}^{opt}_{\boldsymbol{\beta}})_{\boldsymbol{\beta}\in\mathcal{I}}$ in the sense of the Hashin and Shtrikman energy complies with the system

$$\forall\boldsymbol{\beta}\in\mathcal{I},\left(\boldsymbol{\Gamma}_0^c\circledast\boldsymbol{\tau}\right)_{\boldsymbol{\beta}}+(2\mu_{\boldsymbol{\beta}}-2\mu_0)^{-1}\boldsymbol{\tau}_{\boldsymbol{\beta}}=\boldsymbol{d}^{\alpha}_{\boldsymbol{\beta}}.\tag{15}$$

In the case were the pixel averaged viscosity matches the reference viscosity, the polarization is forced to zero on the corresponding pixels.

The quadratic form associated with the Hashin and Shtrikman functional has been shown to be definite positive [18], so the system (15) has a unique solution. To take advantage of the fast evaluation of the discrete convolution product by FFT, the matrix underlying this system is not explicited, although its expression is known through the pixel to pixel interaction terms of the fourth order Green operator. Instead, Brisard and Dormieux [11] suggest using iterative linear solvers such as the conjugate gradient. The optimum bound on the permeability for a given discretization is then

$$\boldsymbol{\alpha}\cdot\boldsymbol{K}\cdot\boldsymbol{\alpha}\leqslant\boldsymbol{\alpha}\cdot\boldsymbol{G}_0^{\mathcal{S}\mathcal{S}}\cdot\boldsymbol{\alpha}-\frac{1}{N}\sum_{\boldsymbol{\beta}\in\mathcal{I}}\boldsymbol{\tau}^{opt}_{\boldsymbol{\beta}}:\boldsymbol{d}^{\alpha}_{\boldsymbol{\beta}}.$$

The average on pixel $\Omega_{\boldsymbol{\beta}}$ of the associated strain rate and velocity fields are

$$\boldsymbol{d}^{opt}_{\boldsymbol{\beta}}=\boldsymbol{d}^{\alpha}_{\boldsymbol{\beta}}-\left(\boldsymbol{\Gamma}_0^c\circledast\boldsymbol{\tau}^{opt}\right)_{\boldsymbol{\beta}},\tag{16a}$$

$$\boldsymbol{v}^{opt}_{\boldsymbol{\beta}}=\left(\boldsymbol{G}_0^{\mathcal{S}\boldsymbol{\beta}}-\boldsymbol{G}_0^{\mathcal{S}\mathcal{S}}\right)\cdot\boldsymbol{\alpha}+\left(\boldsymbol{\mathcal{G}}_0^c\circledast\boldsymbol{\tau}^{opt}\right)_{\boldsymbol{\beta}}-\frac{1}{N}\sum_{\boldsymbol{\delta}\in\mathcal{I}}\boldsymbol{\mathcal{G}}_0^{\mathcal{S}\boldsymbol{\delta}}:\boldsymbol{\tau}^{opt}_{\boldsymbol{\delta}}.\tag{16b}$$

They will be shown to be good approximations of the solution of the initial problem (P^i) in section 4.1. Furthermore, they also prove to be energetically consistent since, recalling the operator $\boldsymbol{\mathcal{G}}$ is anti-symmetric and the previous expression of the bound, the following identity holds

$$\boldsymbol{\alpha}\cdot\boldsymbol{K}\cdot\boldsymbol{\alpha}\leqslant\boldsymbol{\alpha}\cdot\boldsymbol{G}_0^{\mathcal{S}\mathcal{S}}\cdot\boldsymbol{\alpha}+\frac{1}{N}\sum_{\boldsymbol{\beta}\in\mathcal{I}}\boldsymbol{\alpha}\cdot\boldsymbol{\mathcal{G}}_0^{\mathcal{S}\boldsymbol{\beta}}:\boldsymbol{\tau}^{opt}_{\boldsymbol{\beta}}=-\boldsymbol{\alpha}\cdot\frac{1}{N}\sum_{\boldsymbol{\beta}\in\mathcal{I}}\boldsymbol{v}^{opt}_{\boldsymbol{\beta}}.\tag{17}$$

Prepared using nagauth.cls
DOI: 10.1002/nag.2278

3.6. Numerical implementation

The linear system of finite dimension (15) may be formally written $\boldsymbol{A} \cdot \boldsymbol{X} = \boldsymbol{B}$, where

- The vector $\boldsymbol{X}$ contains all the degrees of freedom of the system, that is all the components of the discrete polarization for each of the N pixels (or voxels). For example, in dimension 2,

  $$\boldsymbol{X} = \{\tau_{\boldsymbol{0},11}, \tau_{\boldsymbol{0},22}, \sqrt{2}\tau_{\boldsymbol{0},12}, ..., \tau_{\boldsymbol{\beta},11}, \tau_{\boldsymbol{\beta},22}, \sqrt{2}\tau_{\boldsymbol{\beta},12}, ..., \tau_{\boldsymbol{N-1},11}, \tau_{\boldsymbol{N-1},22}, \sqrt{2}\tau_{\boldsymbol{N-1},12}\},$$

  where the second part of the lowerscript denotes the component of a second order tensor.
- The vector $\boldsymbol{B}$ contains the discretized reference strain rate $\boldsymbol{d}^{\alpha}_{\boldsymbol{\beta}}$. Namely, in dimension 2,

  $$\boldsymbol{B} = \{d^{\alpha}_{\boldsymbol{0},11}, d^{\alpha}_{\boldsymbol{0},22}, \sqrt{2}d^{\alpha}_{\boldsymbol{0},12}, ..., d^{\alpha}_{\boldsymbol{\beta},11}, d^{\alpha}_{\boldsymbol{\beta},22}, \sqrt{2}d^{\alpha}_{\boldsymbol{\beta},12}, ..., d^{\alpha}_{\boldsymbol{N-1},11}, d^{\alpha}_{\boldsymbol{N-1},22}, \sqrt{2}d^{\alpha}_{\boldsymbol{N-1},12}\}.$$

  The discretized reference strain rate needs to be computed only once, at the beginning of the iterative scheme evocated below, as follows

  1. $\{\hat{\chi}^{\mathcal{S}}_{\boldsymbol{b}}...\} = FFT\left(\{\chi^{\mathcal{S}}_{\boldsymbol{\beta}}...\}\right)$
  2. $\forall \boldsymbol{b} \in \mathcal{I}, \hat{\boldsymbol{d}}^{\alpha}_{\boldsymbol{b}} = \left({}^{t}\hat{\boldsymbol{\mathcal{G}}}^{c}_{0}\right)_{\boldsymbol{b}} \cdot f_{\mathcal{S}}^{-1}\hat{\chi}^{\mathcal{S}}_{\boldsymbol{b}}\boldsymbol{\alpha}$
  3. $\{\boldsymbol{d}^{\alpha}_{\boldsymbol{\beta}}...\} = FFT^{-1}\left(\{\hat{\boldsymbol{d}}^{\alpha}_{\boldsymbol{b}}...\}\right)$.
- The matrix $\boldsymbol{A}$, whose components shall not be stored, operates on $\boldsymbol{X}$ as follows

  1. $\{\hat{\boldsymbol{\tau}}_{\boldsymbol{b}}...\} = FFT\left(\{\boldsymbol{\tau}_{\boldsymbol{\beta}}...\}\right)$
  2. $\forall \boldsymbol{b} \in \mathcal{I}, \hat{\boldsymbol{\eta}}_{\boldsymbol{b}} = \left(\hat{\boldsymbol{\Gamma}}^{c}_{0}\right)_{\boldsymbol{b}} : \hat{\boldsymbol{\tau}}_{\boldsymbol{b}}$
  3. $\{\boldsymbol{\eta}_{\boldsymbol{\beta}}...\} = FFT^{-1}\left(\{\hat{\boldsymbol{\eta}}_{\boldsymbol{b}}...\}\right)$
  4. $\forall \boldsymbol{\beta} \in \mathcal{I}, (\boldsymbol{A} \cdot \boldsymbol{X})_{\boldsymbol{\beta}} = \boldsymbol{\eta}_{\boldsymbol{\beta}} + (2\mu_{\boldsymbol{\beta}} - 2\mu_0)^{-1}\boldsymbol{\tau}_{\boldsymbol{\beta}}$.

The matrix $\boldsymbol{A}$ is associated to a definite positive quadratic form. Hence, the system can be inverted using a conjugate gradient (CG) algorithm [19]. The CG is an iterative linear solver which repeatedly improves the vector $\boldsymbol{X}$ until $\boldsymbol{A} \cdot \boldsymbol{X}$ is sufficiently close to $\boldsymbol{B}$ at a precision asked for by the user. Any starting point can be chosen for $\boldsymbol{X}$, such as a vector of zeros. Then, all the CG needs is the right hand side vector $\boldsymbol{B}$ and a method to compute $\boldsymbol{A} \cdot \boldsymbol{X}$ given $\boldsymbol{X}$, but not the matrix $\boldsymbol{A}$ explicitly.

Once the system has been solved for $\boldsymbol{\tau}^{opt}$, the optimal discrete velocity and strain rates fields can be computed using (16), where the discrete convolutions products are evaluated in the Fourier space as in the previous examples. A bound on the permeability is obtained using (17).

4. VALIDATION AND APPLICATION

The Hashin and Shtrikman based FFT method as been implemented in two dimensions (plane strain) and three dimensions, including the three types of both consistent and filtered non consistent Green operators [12]. In this section, we propose a validation of the method by comparison with results from literature and simulations using the Finite Element Method (FEM) code Cast3M on simple geometries which may easily be meshed. Then, an application is proposed as an illustration on a material made of randomly positioned ellipsoids, allowing them to overlap, which has connex fluid and solid phases.

4.1. The problems of the 2D square and circular particles: comparison with FEM

In this validation section, the academic problems a flow past a regular array of square and circular cylinders are numerically studied. The problems are two dimensional (plane strain) and the geometries described on Fig. 1. Note that thanks to the symmetry properties of the geometries considered, the method does not fall in the limitation of the present implementation linked to a possible rotation a the solid phase.

DOI: 10.1002/nag.2278

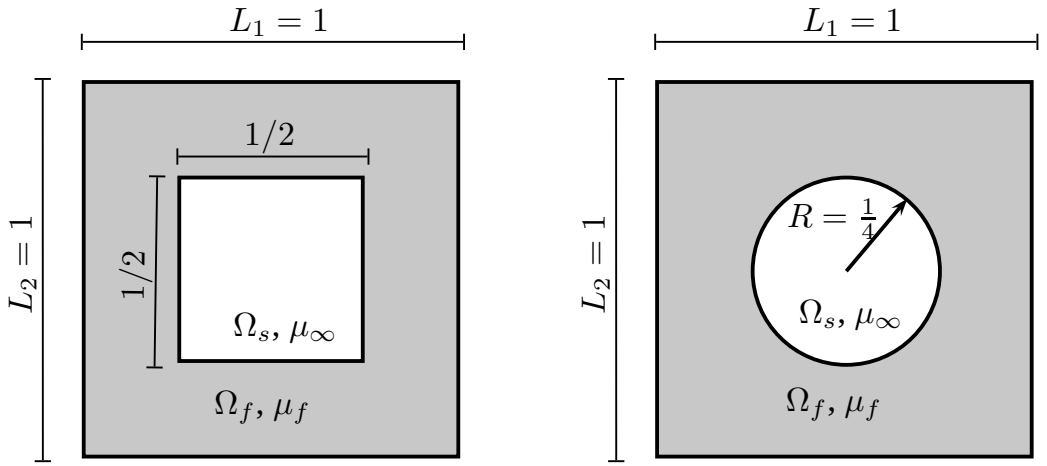

Figure 1. The problems of flow past square (left) and circular (right) cylinders.

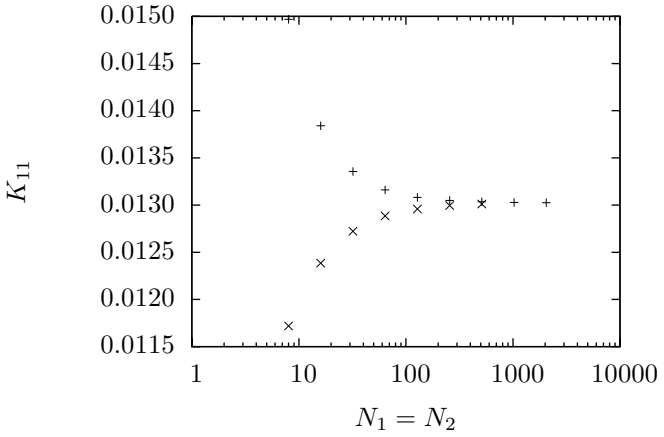

Figure 2. Bounds on the permeability in the problem of the square inclusion, plotted as a function of resolution ($N_1 = N_2$ is the number of pixels along each side of the domain). In this application, $\mu_0 = \mu_f = 1$. FEM results ($\times$) have been carried out using quadratic square-shaped elements on a regular grid and provide lower bound estimates, while FFT based results ($+$) provide upper bound estimates.

The viscosity of the fluid is taken to $\mu_f = 1$ and the macroscopic pressure gradient is set to $\boldsymbol{\alpha} = \boldsymbol{e}_1$, so that the bound is obtained on the component K_{11} of the intrinsic permeability tensor. FEM computations have been carried out in linear elasticity using quadratic elements. The no velocity boundary condition is directly prescribed at the solid - fluid interphase as a no displacement condition.

For the FFT computations in the square cylinder problem, the reference viscosity is chosen equal to the fluid velocity, so that only the solid phase is polarized. This choice experimentally provides the best bound for a given discretization. Note that this is valid only for geometries in which the viscosity averaging rule need is not needed. This choice also results in less iterations of the linear iterative solver, since the space of explored polarization fields is shrunk. The solid phase is associated to a fluid of infinite viscosity μ_∞, and the choice $\Omega_{\mathcal{S}} = \Omega_s$ is made. Consistent discrete Green operators have been used in this example.

DOI: 10.1002/nag.2278

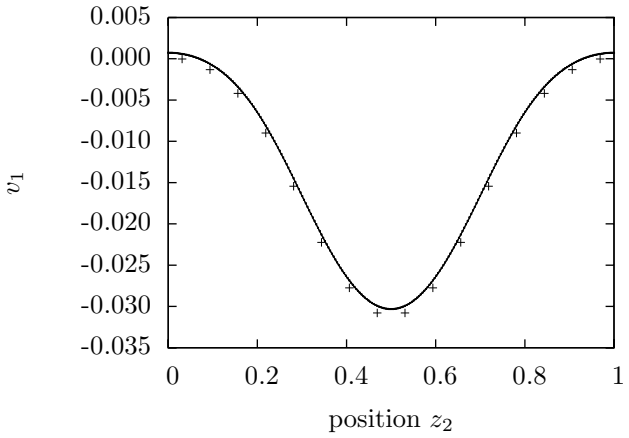

Figure 3. Local values of the v_1 component of the velocity field along the right boundary of the domain Ω. Displayed FEM results are the 257 nodal displacements of a simulation carried out using quadratic square-shaped elements on a regular 256×256 grid. Displayed FFT results are average velocities on a pixel. FFT results on the 1024×1024 grid may hardly be distinguished from the FEM results. FFT results on the poorly discretized 16×16 grid (+) still provide a close approximation.

Results for the bound on K_{11} are shown in Fig. 2. Since the FEM method is based on the principle of the minimum potential energy (6), refinement of the meshing grid provides increasingly closer lower bounds on the permeability. On the contrary, the Hashin and Shtrikman based FFT method Eq. (14) has been proved to provide increasingly closer upper bounds with grid refinement. Both method steadily converge to the same value.

The local velocities and strains computed using (16) prove to be good approximations of the solution velocity fields on Fig. 3, even for a low discretization grid (16×16). These observations also holds for the strain rate field. Careful look shows the local velocities computed using the FFT scheme tend to overestimate the flow in the direction of the gradient of permeability, which is coherent with the upper bound status of the method. Velocities in the solid phase are not exactly null, but several orders of magnitude lower than in the fluid phase, depending on the grid refinement.

The circular cylinder problem is slightly more involved to deal with using the FFT based scheme, since the solid fluid interphase does not coincide with pixel boundaries. First, the viscosity averaging rule requires the knowledge of the volume fractions of the solid phase in every pixel, which is not straight forwardly computed for this particular geometry. We thus consider the approximate problem of a rough disc discretized on a high resolution 2048×2048 grid. Then, this problem is discretized on lower resolution grids using the viscosity averaging rule to be solved.

Second, the choice of the reference viscosity is not obvious. Indeed, choosing the reference viscosity equal to the fluid viscosity causes the viscosity averaging rule to degenerate. Namely, the equivalent viscosity is equal to the fluid viscosity in the case of a pixel comprising both fluid and solid. However, this choice would still result on an upper bound on the permeability. On the other hand, choosing the reference viscosity too far from the fluid viscosity provides worsening estimates. To sum up, in this case the reference medium has to be chosen different from the fluid to properly capture the solid fluid interphase, but not too far to provide good estimates. The influence of the choice of reference medium is shown on Fig. 4. The optimum reference viscosity value does not dramatically improve the bound as compared with the choice $\mu_0 = \mu_f = 1$ in this specific example. However, it is believed to be crucial for real microstructure whose volume fraction of heterogeneous pixels is more important. No theoretical argument has yet been found to optimize the choice of the reference medium. One must also take into account

DOI: 10.1002/nag.2278

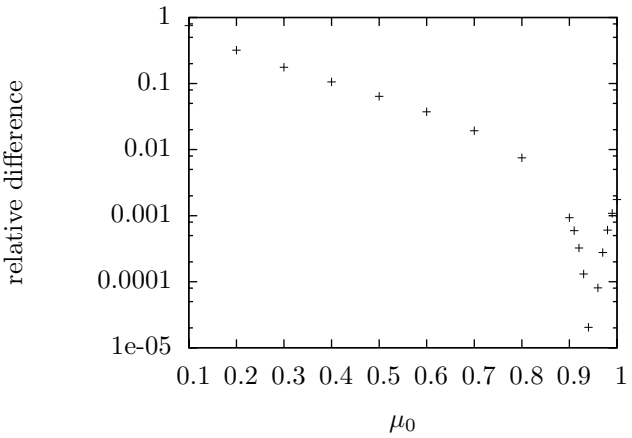

Figure 4. Influence of the choice of reference medium on the bound. Computation have been carried out in a 128×128 grid for the rough circular inclusion previously discretized on a 2048×2048 grid. The reference for the relative difference is the value obtained for the choice $\mu_0 = 0.95$ which provided the lowest upper bound for the 128×128 optimization grid.

that the linear system to be solved becomes ill conditioned for choices of the reference viscosity too close from local viscosities.

Comparison of the bound on the permeability and the local fields obtained by FFT with FEM results showed closely converging results, similar to the square cylinder inclusion results.

4.2. The problems of the 3D cubic and spherical particles: comparison with FEM and literature

The problem of the flow past a cubic particle is the exact three dimensional counterpart of the previous two dimensional square inclusion problem. In order to validate the implementation of the method in three dimensions, comparison has been made with FEM simulations using the same set of parameters as in the previous section. The results are not exposed in this paper since they show exactly the same trend as in the two dimensions implementation. Namely, the estimates on the permeability steadily converge to the same value and the local velocity and strain rates fields are in excellent agreement.

Another convincing validation is the comparison with the results of Sangani and Acrivos [20], Jung and Torquato [21], and Wiegmann [8] for arrays of disjoint spheres and Tardif d'Hamonville [16] for arrays of interpenetrating spheres. Tardif d'Hamonville carried out simulations of a Stokes flow past periodic cubic arrays of spheres using a FEM code specially designed to manage the difficulties arising from the fluid incompressibility. For the FFT computations, the spheres are first discretized on a 8192^3 grid to estimate the solid volume fractions of the heterogeneous pixels. Then, computations are carried out on 64^3 and 128^3 grids and compared to existing results on Fig. 5. For these computations, $\Omega_{\mathcal{S}}$ is chosen as the set of pixels having an infinite equivalent viscosity after application of the viscosity averaging rule and the reference viscosity as three quarters of the fluid viscosity.

The method proves to yield accurate results over a large range of sphere radii. The precision of the results are compared with the previous work of Sangani and Acrivos [20], Jung and Torquato [21], and Wiegmann [8] on Fig. 6. Our results on a low discretization grid benefit from the viscosity averaging rule for the proper description of the solid fluid boundary. The relative error appears to converge faster with grid refinement than for the method proposed by Wiegmann [8].

DOI: 10.1002/nag.2278

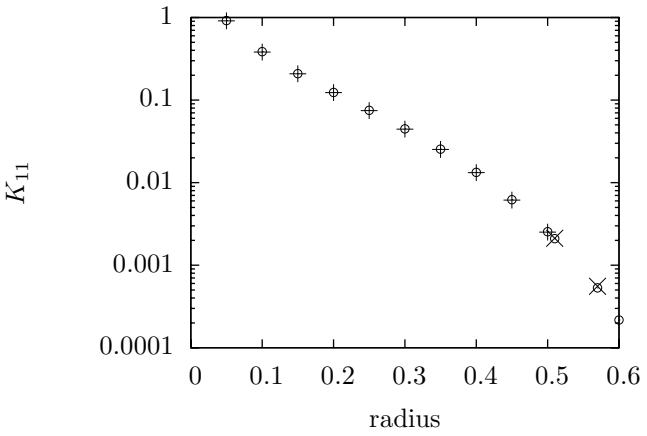

Figure 5. Evolution of the permeability of an array of spheres as a function of the radius. FFT computations have been carried out on a 128^3 grid for a rough spherical inclusion previously discretized on a 8192^3 grid. FFT results ($\odot$) compare well with the reference work of Sangani and Acrivos [20] ($+$) and Tardif d'Hamonville [16] ($\times$).

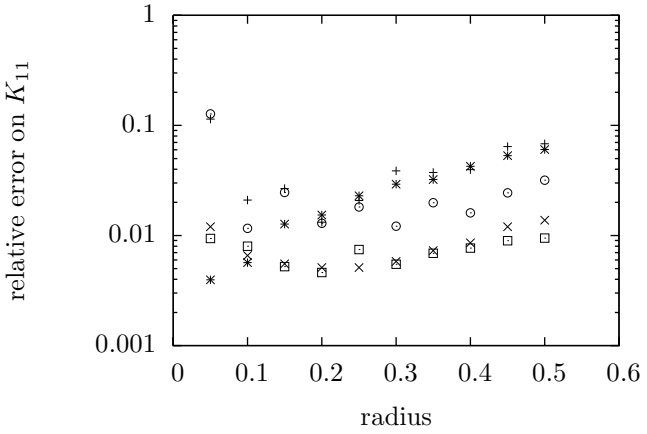

Figure 6. Relative error on the permeability of an array of spheres as compared to the reference work of Sangani and Acrivos [20] as a function of the radius. FFT computations have been carried out on 64^3 ($\odot$) and 128^3 ($\boxdot$) grids for a rough spherical inclusion previously discretized on a 8192^3 grid. Relative errors are presented for comparison from the results of Jung and Torquato [21] ($*$) and Wiegmann [8] on 40^3 ($+$) and 240^3 ($\times$) grids.

4.3. Application : flow through random overlapping ellipsoids

The numerical method is now applied to a computer made material, taken as a more realistic example of a granular material. The solid phase is made of randomly positioned and oriented ellipsoidal grains. The grains are allowed to overlap, so that the solid phase is connex. In the studied range of porosity, the connexity of the solid and fluid phase has been checked using the 3d image processing software ImageJ.

Simulations have been run on a 256^3 voxels periodic cell made of 200 oblate ellipsoids with half great axis 32 voxels and half small axis 16 voxels. The size of the cell is 1 unit length in each direction. The porosity is 44.1% and the fluid viscosity is 1. The microstructure and an example of computed velocity field are displayed on Fig. 7.

DOI: 10.1002/nag.2278

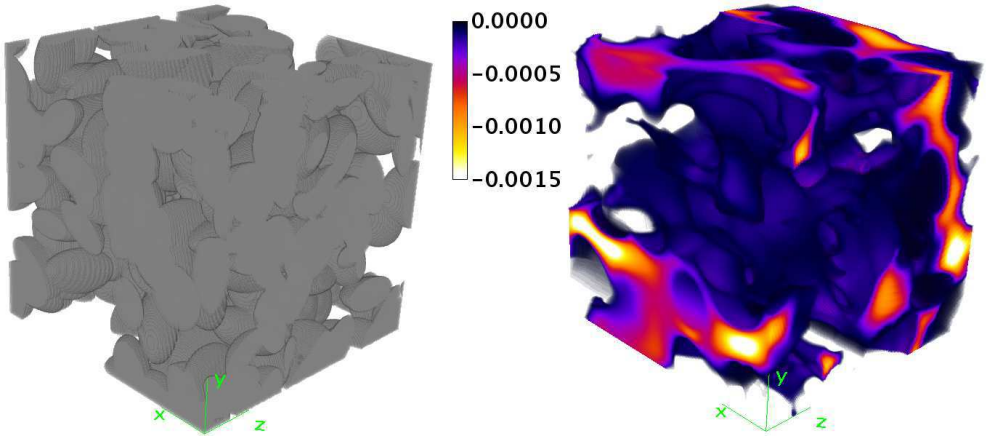

(a) solid phase (b) velocity

Figure 7. Simulations on a unit size box of 256^3 voxels. (a) The solid phase, in gray, is made of 200 randomly positioned and oriented oblate ellipsoids with major axis 64 pixels and aspect ratio of 2. (b) Local values of the v_1 component of the velocity field for a unit pressure gradient $\boldsymbol{\alpha} = \boldsymbol{e}_1$ and fluid viscosity of 1. Low velocity areas (solid phase) have been set transparent.

For this cell, the computed permeability tensor, expressed in the cell basis in length unit square is

$$\begin{bmatrix} 1.432 \times 10^{-4} & 0.073 \times 10^{-4} & 0.047 \times 10^{-4} \\ 0.073 \times 10^{-4} & 1.466 \times 10^{-4} & -0.053 \times 10^{-4} \\ 0.047 \times 10^{-4} & -0.052 \times 10^{-4} & 1.019 \times 10^{-4} \end{bmatrix}$$

As expected, the permeability tensor is symmetric. However, the tensor is observed to be not exactly isotropic, whereas the grains orientation is random. This result indicates the cell is not quite large enough to be considered as a representative volume element of such random material. In future works, such representativity considerations will have to be taken into account for computations on real microstructures obtained from imaging techniques, irrespective of the simulation method used.

5. CONCLUSION

The present work introduced a Hashin and Shtrikman variational framework for the darcean flow problem with periodic boundary conditions. This formulation proved to be a solid basis for the development of numerical approximate solutions. As a by-product, a field of new considerations is opened for approximate analytical solutions following existing work in linear elasticity. The variational framework ensures the status of upper bound on the permeability of any derived estimate.

The proposed method is computationally faster than FEM and much easier to implement. Furthermore, no meshing operation has to be realized, since images may be directly used as an input. The variational framework ensures the status of rigorous upper bound of the estimates, as well as an improvement of the estimates with grid refinement, and a consistent way of dealing with pixels crossed by the solid - fluid boundary.

Future work will consist in comparing the method to experimental results on real materials.

ACKNOWLEDGEMENT

DOI: 10.1002/nag.2278

The authors thanks Sébastien Brisard for kindly providing its implementation of the Hashin and Shtrikman FFT-based code in linear elasticity. He also helped making it easily compatible with the permeability counterpart and gave useful analytical and programming tips.

A. ON THE DIFFERENT ORDER GREEN OPERATORS

The second order Green operator, called Green function $\boldsymbol{G}_0$, solves for the velocity $\boldsymbol{u}$ in a RVE Ω comprising a uniform material with linear properties loaded by a body force field $\boldsymbol{f}$ through

$$\boldsymbol{u}(\boldsymbol{z}) = \int_\Omega \boldsymbol{G}_0(\boldsymbol{z},\boldsymbol{y}) \cdot \boldsymbol{f}(\boldsymbol{y}) \,\mathrm{d}\, V_y = (\boldsymbol{G}_0 * \boldsymbol{f})\,(\boldsymbol{z}). \tag{18}$$

In the Fourier space, the convolution product in (18) is simply expressed as a dot product

$$\hat{\boldsymbol{u}}(\boldsymbol{k}) = \hat{\boldsymbol{G}}_0(\boldsymbol{k}) \cdot \hat{\boldsymbol{f}}(\boldsymbol{k}),$$

where the following notations are used for the Fourier space: $\boldsymbol{k}$ is the wave vector, $\boldsymbol{n}$ its normalization, $\hat{f}$ the Fourier transform of a function f.

Following a reasoning similar to [22, Appendix A], using periodic boundary conditions and solving in the Fourier space, the Green function appears to be the inverse of the acoustic tensor, so that its components are known except in $\boldsymbol{k} = 0$ by

$$\hat{\boldsymbol{G}}_0(\boldsymbol{k}) = \frac{1}{\mu_0 |k|^2} \left(\boldsymbol{I} - \frac{1}{2(1-\nu_0)} \boldsymbol{n} \otimes \boldsymbol{n} \right).$$

For the sake of a direct link with linear elasticity, the Poisson coefficient ν_0 is introduced, keeping in mind that it is equal to one half in the case of an incompressible fluid. μ_0 would be the shear modulus in linear elasticity but must here be considered as a viscosity. For $\boldsymbol{k} = \boldsymbol{0}$ the convention is the operators are null. The Green function is symmetrical.

A third order Green operators may be defined. This operator links polarization to velocity through $\boldsymbol{v} = \boldsymbol{\mathcal{G}}_0 * \boldsymbol{\tau}$ and is expressed as

$$\hat{\boldsymbol{\mathcal{G}}}_0(\boldsymbol{k}) = -\imath \hat{\boldsymbol{G}}_0(\boldsymbol{k}) \overset{s}{\otimes} \boldsymbol{k},$$

where the superscript s indicates symmetrization. Then body forces are linked to strain rates through $\boldsymbol{d} =^t \boldsymbol{\mathcal{G}}_0 * \boldsymbol{f}$. Use of the Maxwell-Betti theorem indicates that the operator $\boldsymbol{\mathcal{G}}_0$ is anti-symmetric in the sense

$$\overline{\boldsymbol{f} \cdot (\boldsymbol{\mathcal{G}}_0 * \boldsymbol{\tau})} = -\overline{\boldsymbol{\tau} : ({}^t\boldsymbol{\mathcal{G}}_0 * \boldsymbol{f})}.$$

The fourth order Green operator $\boldsymbol{\Gamma}_0$ has already been discussed by authors (eg. [22]) in the periodic context and links the polarization to strain rate through $\boldsymbol{d} = -\boldsymbol{\Gamma}_0 * \boldsymbol{\tau}$. It may be expressed in Fourier space as

$$\hat{\boldsymbol{\Gamma}}_0(\boldsymbol{k}) = -\boldsymbol{k} \overset{s}{\otimes} \hat{\boldsymbol{G}}_0(\boldsymbol{k}) \overset{s}{\otimes} \boldsymbol{k}.$$

B. ON DISCRETIZED PERIODIC GREEN OPERATORS

The periodized Green operator introduced in [11] and extensively discussed in [12] may be generalized to different order operators. Consider an operator $\mathcal{H}$ operating as $\boldsymbol{x}(\boldsymbol{z}) = (\mathcal{H} * \boldsymbol{y})\,(\boldsymbol{z})$ and two subdomains Ω_I and Ω_J of Ω whose characteristic functions are denoted χ^I and χ^J, of volume fractions f_I and f_J. Following the work of Molinari and El Mouden [23] to capture the interaction of elastic inclusions, we introduce the interaction term:

$$\mathcal{H}^{IJ} = \overline{f_I^{-1} \chi^I \mathcal{H} * f_J^{-1} \chi^J}.$$

Physically speaking, the interaction term $\mathcal{H}^{IJ}$ yields the average velocity (or strain) on domain Ω^I resulting from a uniform body force (or polarization) applied on domain Ω^J, depending on the choice of Green operator. Using the properties of the Fourier transform,

$$\mathcal{H}^{IJ} = f_I^{-1} f_J^{-1} \sum_{\boldsymbol{b} \in \mathbb{Z}^d} \hat{\chi}^{I^*}(\boldsymbol{k_b}) \hat{\mathcal{H}}(\boldsymbol{k_b}) \hat{\chi}^J(\boldsymbol{k_b}),$$

Prepared using nagauth.cls
DOI: 10.1002/nag.2278

where the superscript $*$ denotes the complex conjugate. Note that the influence term is null if Ω_I or Ω_J is equal to Ω in the case of Green operators, since they are null for $\boldsymbol{k} = \boldsymbol{0}$.

Now assume Ω_I and Ω_J are both a union of pixels, as defined in section 3.5. The finite data series $(\chi^I_{\boldsymbol{\beta}})_{\boldsymbol{\beta}\in\mathcal{I}}$ is introduced, such as $\chi^I_{\boldsymbol{\beta}} = 1$ if the pixel Ω_β is in Ω_I, and is null otherwise. For this particular choice, the Fourier transform of $\hat{\chi}^I(\boldsymbol{k_b})$ is linked to the discrete Fourier transform (DFT) $\hat{\chi}^I_{\boldsymbol{b}}$ by

$$\hat{\chi}^I(\boldsymbol{k_b}) = \left[\prod_{c\in(1,..,d)} \frac{1}{N_c}\,\mathrm{sinc}\left(\frac{\pi b_c}{N_c}\right)\right]\hat{\chi}^I_{\boldsymbol{b}}.$$

Reorganizing the sum over $\mathbb{Z}^d$ to take advantage of the DFT periodicity leads to the introduction of the consistently discretized operator $\hat{\mathcal{H}}^c$ in the Fourier space

$$\hat{\mathcal{H}}^{\mathfrak{c}}_{\boldsymbol{b}} = \sum_{\boldsymbol{n}\in\mathbb{Z}^d}\left[\prod_{c\in(1,..,d)} \mathrm{sinc}\left(\frac{\pi b_c}{N_c}\right)\right]^2 \hat{\mathcal{H}}(\boldsymbol{k}_{b_1+n_1N_1,\ldots,b_d+n_dN_d}),$$

in order to express the influence term as

$$\mathcal{H}^{IJ} = \frac{1}{N^2 f_I f_J}\sum_{\boldsymbol{b}\in\mathcal{I}} \hat{\chi}^{I^*}_{\boldsymbol{b}}\hat{\mathcal{H}}^c_{\boldsymbol{b}}\hat{\chi}^J_{\boldsymbol{b}}.$$

A discrete convolution product $\circledast$ may be defined by introducing the sequence $\left(\mathcal{H}^c \circledast \chi^J\right)_{\boldsymbol{\beta}}$ whose DFT is

$$\widehat{\left(\mathcal{H}^c \circledast \chi^J\right)}_{\boldsymbol{b}} = \hat{\mathcal{H}}^c_{\boldsymbol{b}}\hat{\chi}^J_{\boldsymbol{b}}.$$

Use of the Plancherel theorem provides the useful relation

$$\mathcal{H}^{IJ} = \frac{1}{N f_I f_J}\sum_{\boldsymbol{\beta}\in\mathcal{I}} \chi^I_{\boldsymbol{\beta}}\left(\mathcal{H}^c \circledast \chi^J\right)_{\boldsymbol{\beta}} = \frac{1}{N f_I f_J}\sum_{\boldsymbol{\beta}\in\mathcal{I}} \chi^J_{\boldsymbol{\beta}}\left(\mathcal{H}^c \circledast \chi^I\right)_{\boldsymbol{\beta}}.$$

Thus, the convolution products may be exactly computed if Ω_I and Ω_J are both a union of pixels thanks to the relation

$$\overline{\chi_I\mathcal{H} * \chi_J} = \frac{1}{N}\sum_{\boldsymbol{\beta}\in\mathcal{I}} \chi^I_{\boldsymbol{\beta}}\left(\mathcal{H}^c \circledast \chi^J\right)_{\boldsymbol{\beta}},$$

where the discrete convolution product may be numerically computed by FFT of $(\chi^J_{\boldsymbol{\beta}})_{\boldsymbol{\beta}\in\mathcal{J}}$, product with the consistent operator in the Fourier space and inverse FFT.

The consistent operators require computation of infinite sums. The rate of convergence of these sums is slow for the fourth order Green operator but faster for the second and third order Green operators. The sums may be computed once and stored for usual discretization grids. For sufficiently refined grids, [12] proved they could be advantageously replaced by so-called filtered non consistent operators in a very satisfactory approximation, which neither require involved computations nor storage.

REFERENCES

1. Ene H, Sanchez-Palencia E. Equations et phénomènes de surface pour l'écoulement dans un modèle de milieu poreux. *Journal de Mécanique* 1975; :73–108.
2. Boutin C. Study of permeability by periodic and self-consistent homogenisation. *European Journal of Mechanics A/Solids* 2000; **19**:603–632.
3. Boutin C, Geindreau C. Estimates and bound of dynamic permeability of granular media. *Journal of the Acoustical Society of America* 2008; **124**(6):3576–3593.
4. Blunt MJ, Jackson MD, Piri M, Valvatne PH. Detailed physics, predictive capabilities and macroscopic consequences for pore-network models of multi-phase flow. *Advances in Water Ressources* 2002; **25**:1069–1089.
5. Desbois G, Urai JL, Kukla PA, Konstanty J, Baerle C. High-resolution 3d fabric and porosity model in a tight gas sandstone reservoir: A new approach to investigate microstructures from mm- to nm-scale combining argon beam cross-sectioning and sem imaging. *Journal of Petroleum Science and Engineering* 2011; **78**:243–257.
6. Tölke J, Baldwin C, Mu Y, Fang NDQ, Grader A, Dvorkin J. Computer simulations of fluid flow in sediment: from images to permeability. *The Leading Edge* January 2010; :68–74.

DOI: 10.1002/nag.2278

7. Bernard D, Nielsen O, Salvo L, Cloetens P. Permeability assessment by 3d interdentritic flow simulations on microtomography mappings of al-cu alloys. *Materials Science and Engineering* 2005; **392**:112–120.
8. Wiegmann A. Computation of the permeability of porous materials from their microstructure by fff-stokes. *Berichte des Fraunhofer ITWM* 2007; **129**.
9. Moulinec H, Suquet P. A fast numerical method for computing the linear and non linear properties of composites. *Comptes Rendus de l'Académie des Sciences* 1994; **2**(318):1417–1423.
10. Monchiet V, Bonnet G, Lauriat G. A fft-based method to compute the permeability induced by a stokes slip flow through a porous medium. *Comptes Rendus de Mécanique* 2009; **337**:192–197.
11. Brisard S, Dormieux L. Fft-based methods for the mechanics of composites: A general variational framework. *Computational Materials Science* 2010; **49**:663–671.
12. Brisard S, Dormieux L. Combining galerkin approximation techniques and the principle of hashin and shtrikman to improve two fft-based numerical methods for the homogenization of composites. *Computer Methods in Applied Mechanics and Engineering* 2012; **217-220**:197–212.
13. Auriault JL. Upscaling heterogeneous media by asymptotic expansions. *Journal of Engineering Mechanics* 2002; **128**(8):817–822.
14. Dormieux L, Kondo D, Ulm FJ. *Microporomechanics*. Wiley, 2006.
15. Auriault JL, Sanchez-Palencia E. Etude du comportement macroscopique d'un milieu poreux saturé déformable. *Journal de Mécanique* 1977; **16**:575–603.
16. Tardif-d'Hamonville P. Modélisation et simulation du transport advectif et diffusif en milieu poreux monophasique et diphasique. PhD Thesis, École Nationale des Ponts et Chaussées 2006.
17. Hashin Z, Shtrikman S. On some variational principles in anisotropic and nonhomogeneous elasticity. *Journal of the Mechanics and Physics of Solids* 1962; **10**(4):335–342.
18. Willis J. Bounds and self-consistant estimates for the overall properties of anisotropic composites. *Journal of the Mechanics and Physics of Solids* 1977; **25**:185–202.
19. Barrett R, Berry M, Chan TF, Demmel J, Donato J, Dongarra J, Eijkhout V, Pozo R, Romine C, der Vorst HV. *Templates for the Solution of Linear Systems: Building Blocks for Iterative Methods, 2nd Edition*. SIAM: Philadelphia, PA, 1994.
20. Sangani A, Acrivos A. Slow flow through a periodic array of spheres. *International Journal of Multiphase Flow* 1982; **8**:343–360.
21. Jung Y, Torquato S. Fluid permeabilities of triply periodic minimal surfaces. *Physical Review* 2005; **72**(5).
22. Moulinec H, Suquet P. A numerical method for computing the overall response of nonlinear composites with complex microstructure. *Computational Methods in Applied Mechanical Engineering* 1998; **157**:69–94.
23. Molinari A, El-Mouden M. The problem of elastic inclusions at finite concentration. *International Journal of Solids and Structures* 1996; **33**(20-22):3131–3150.

DOI: 10.1002/nag.2278